A&A 560, A46 (2013)
DOI: 10.1051/0004-6361/201322586
© ESO 2013

Astronomy & Astrophysics

GIANO-TNG spectroscopy of red supergiants in the young star cluster RSGC2⋆

L. Origlia[1], E. Oliva[2], R. Maiolino[3], A. Mucciarelli[4], C. Baffa[2], V. Biliotti[2], P. Bruno[5], G. Falcini[2], V. Gavriousev[2], F. Ghinassi[6], E. Giani[2], M. Gonzalez[6], F. Leone[7], M. Lodi[6], F. Massi[2], P. Montegriffo[1], I. Mochi[8], M. Pedani[6], E. Rossetti[4], S. Scuderi[5], M. Sozzi[2], and A. Tozzi[2]

[1] INAF – Osservatorio Astronomico di Bologna, via Ranzani 1, 40127 Bologna, Italy
e-mail: livia.origlia@oabo.inaf.it
[2] INAF – Osservatorio Astrofisico di Arcetri, Largo E. Fermi 5, 50125 Firenze, Italy
[3] University of Cambridge, Cavendish Lab., JJ Thomson Av., Cambridge CB3 0HE, UK
[4] University of Bologna, Physics & Astronomy Dept., Viale Berti Pichat 6-2, 40127 Bologna, Italy
[5] INAF – Osservatorio Astrofisico di Catania, via S. Sofia 78, 95123 Catania, Italy
[6] INAF – TNG, ORM Astronomical Observatory, 38787 Garafia, TF, Spain
[7] University of Catania, Physics & Astronomy Dept. via S. Sofia 78, 95123 Catania, Italy
[8] Lawrence Berkeley National Laboratory, 1 Cyclotron Road, MS 2-400, Berkeley CA 94720, USA

Received 2 September 2013 / Accepted 4 November 2013

ABSTRACT

Aims. The inner disk of the Galaxy has a number of young star clusters dominated by red supergiants that are heavily obscured by dust extinction and observable only at infrared wavelengths. These clusters are important tracers of the recent star formation and chemical enrichment history in the inner Galaxy.
Methods. During the technical commissioning and as a first science verification of the GIANO spectrograph at the Telescopio Nazionale *Galileo*, we secured high-resolution ($R \simeq 50\,000$) near-infrared spectra of three red supergiants in the young Scutum cluster RSGC2.
Results. Taking advantage of the full YJHK spectral coverage of GIANO in a single exposure, we were able to identify several tens of atomic and molecular lines suitable for chemical abundance determinations. By means of spectral synthesis and line equivalent width measurements, we obtained abundances of Fe and other iron-peak elements such as V, Cr, Ni, of alpha (O, Mg, Si, Ca and Ti) and other light elements (C, N, Na, Al, K, Sc), and of some s-process elements (Y, Sr). We found iron abundances between half and one third solar and solar-scaled [X/Fe] abundance patterns of iron-peak, alpha and most of the light elements, consistent with a thin-disk chemistry. We found a depletion of [C/Fe] and enhancement of [N/Fe], consistent with CN burning, and low $^{12}C/^{13}C$ abundance ratios (between 9 and 11), requiring extra-mixing processes in the stellar interiors during the post-main-sequence evolution. Finally, we found a slight [Sr/Fe] enhancement and a slight [Y/Fe] depletion (by a factor of ≤2), with respect to solar.

Key words. techniques: spectroscopic – supergiants – stars: abundances – infrared: stars

1. Introduction

High-resolution spectroscopy in the near-infrared (NIR) is a powerful tool for measuring chemical abundances of cool giant and supergiant stars. It is especially critical in very reddened environments such as the inner Galaxy, where extinction is so severe as to prevent any reliable measurement at shorter wavelengths.

Recently, our team made the first technical commissioning of GIANO, a cross-dispersed NIR spectrograph for the Telescopio Nazionale *Galileo* (TNG) at the Roque de Los Muchachos Observatory in La Palma (Spain). GIANO delivers a spectrum that covers in a single exposure the wavelength range from 0.95 μm to 2.4 μm at a resolving power $R \simeq 50\,000$. The main disperser is a commercial R2 echelle grating with 23.2 lines/mm working in quasi-Littrow configuration on a $d = 100$ mm collimated beam. Cross dispersion is achieved via a network of fused silica and ZnSe prisms that work in double pass, that is, they cross-disperse the light both before and after it is dispersed by the echelle gratings, thus producing curved spectral orders. The echellogram on the $2k \times 2k$ detector spans 49 orders, from #32 to #80. The spectral coverage is complete up to 1.7 μm. At longer wavelengths the orders become larger than the detector. The effective spectral coverage in the K-band is about 75%. Light from the telescope feeds a bundle of two IR-transmitting ZBLAN fibers, with a core of 85 μm, corresponding to a sky-projected angle of 1 arcsec. The two fibers are aligned and mounted inside a custom connector. The cores are at a distance of 0.25 mm, equivalent to a sky-projected angle of about 3 arcsec.

Owing to the constraints set by the visitor focus, the fiber entrance was coupled to the TNG using a provisional, simplified focal adapter that consisted of a commercial CaF_2 singlet lens positioned 26 mm before the fibers. The focal adapter was mechanically mounted at a fiducial position, no further adjustment of the optical axis was possible. This unfortunately resulted in a very reduced efficiency of the system, and only bright targets were observable at that time. More technical details on the instrument can be found in Oliva et al. (2012a,b, 2013).

As a first science verification of the GIANO performances, we observed three bright red supergiants (RSGs) in the star cluster RSGC2. RSGC2 is one of the few young, massive (4×10^4 $M_\odot$) clusters in the Galactic plane, located at the base of

⋆ Table 3 is available in electronic form at http://www.aanda.org

Table 1. RSG stars observed with GIANO.

Ref	D09 Ref	ID	RA (J2000)	Dec (J2000)	SpT	J	H	K	A_K	RV (km s^{-1})
#1	#6	J18391838-0600383	18 39 18.386	–06 00 38.39	M5I	7.717	5.919	5.072	1.17	107.1
#2	#2	J18391961-0600408	18 39 19.616	–06 00 40.83	M3I	6.899	5.045	4.120	1.39	111.1
#3	#3	J18392461-0602138	18 39 24.611	–06 02 13.80	M4I	7.273	5.458	4.499	1.34	110.5

Notes. Identification names, coordinates, and magnitudes are taken from 2MASS, reddening A_K and radial velocities are taken from Davies et al. (2007).

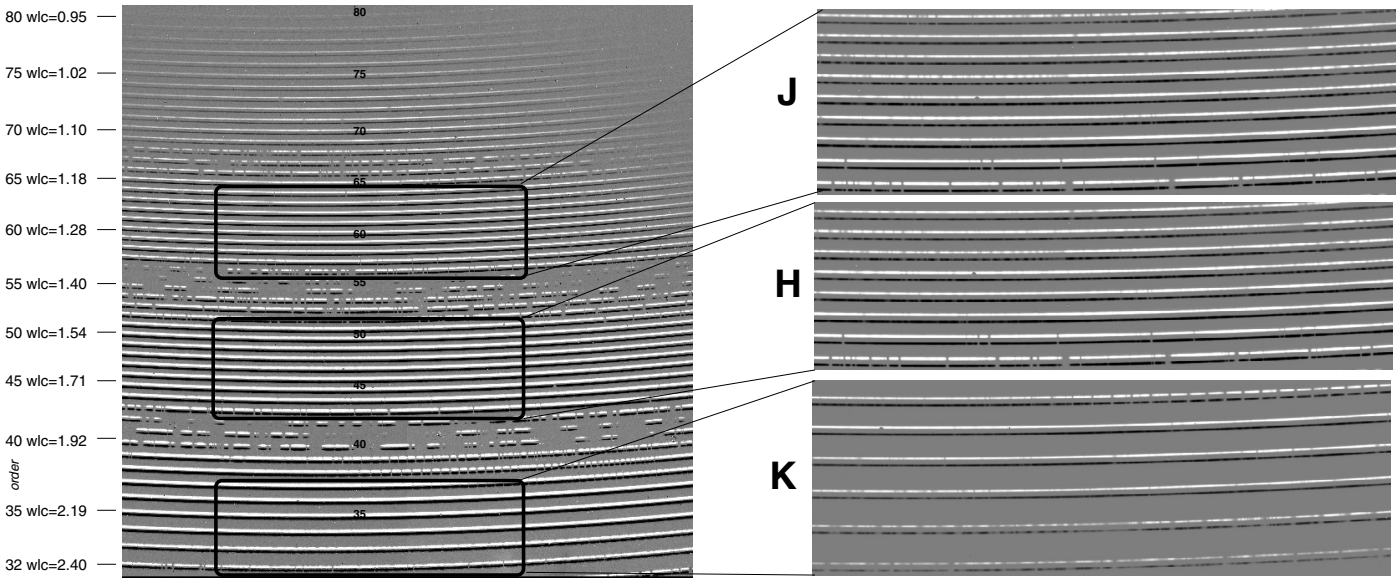

Fig. 1. GIANO 2D (sky-subtracted) spectra of one of the observed RSG stars. Sky subtraction has been performed by nodding on fiber, resulting in one positive and one negative spectrum.

the Scutum-Crux arm and at the tip of the Galactic bar (Davies et al. 2007) at a distance of ≃3.5 kpc from the Galactic center. Such rare clusters are rich in RSG stars and represent ideal laboratories for studying the evolution of massive stars as well as for physically and chemically characterizing the most recent and violent star formation events in the inner Galaxy. However, one can only study them in the IR or at radio wavelengths, because of high visual extinction ($A_V \approx 10$–30 mag) that affects the Galactic plane. Chemical abundances of Fe, C, and alpha-elements have been measured in 12 RSG stars, members of RSGC2, by using medium-resolution ($R \simeq 17\,000$) spectra obtained with NIRSPEC at the KeckII Telescope (Davies et al. 2009b, hereafter D09). In some of these RSGs Verheyen et al. (2012) also found SiO maser emission.

We present and discuss the main atomic and molecular lines identified in the GIANO spectra of the observed three RSGs, which are members of the RSGC2 star cluster and are in common with the D09 sample. We also report the inferred chemical abundances of CNO and F from molecular lines, iron-peak, alpha, and other light elements and a few s-process elements from atomic lines.

2. Observations and data reduction

For the observed targets, the 2MASS reference name, coordinates, spectral type and magnitudes, reddening and radial velocities from Davies et al. (2007) are reported in Table 1.

The reddening estimates do not affect the line equivalent width measurements since at NIR wavelengths the continuum is still dominated by the stellar photosphere and reddening dilutes both the line and the adjacent continuum flux by the same amount.

The data were collected during the technical night on July 30, 2012. A first exposure of 5 min was acquired by centering the star+sky on fiber #1 and the sky alone on fiber #2. Then we acquired a second exposure with the same integration time but with star+sky on fiber #2 and the sky alone on fiber #1 by nodding the telescope. By subtracting the 2D spectrum of the second exposure from the 2D spectrum of the first exposure we obtained the pure star spectrum (see Fig. 1). Nodding on fiber is very effective to properly subtract sky emission and instrumental background. The geometry of the orders was determined using flat exposures with a tungsten calibration lamp. The 2D spectrum was thus rectified and the spectra from each order were extracted by summing six pixels around each fiber, in the direction perpendicular to dispersion. Wavelength calibration was determined by feeding the fibers with the light from a U-Ne lamp. The wavelengths of the uranium lines were taken from Redman et al. (2011), while for neon we used the table available on the NIST (Kramida et al. 2012). The λ versus pixel relationship was obtained starting from a physical model of the instrument. This procedure is part of the pipeline that we are developing for the instrument. The resulting wavelength accuracy was about $\lambda/300\,000$ rms, that is, 0.05 Å for lines in the H-band, while the overall signal-to-noise ratio is about 50. For the three observed stars we found radial velocities consistent with the values reported by Davies et al. (2007) and listed in Table 1.

Figure 2 shows a few examples of the observed spectra for iron-peak and s-process elements, Fig. 3 for alpha elements and Fig. 4 for other light elements.

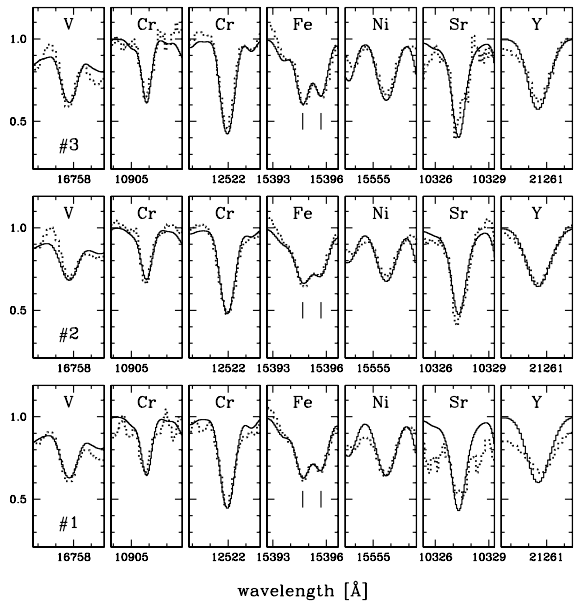

Fig. 2. GIANO spectra around some iron-peak and s-process element lines for the three observed RSG stars (dotted lines). Our best-fit models are overplotted as solid lines. Rest frame wavelengths are defined in air and thickmarks are every Å in each panel.

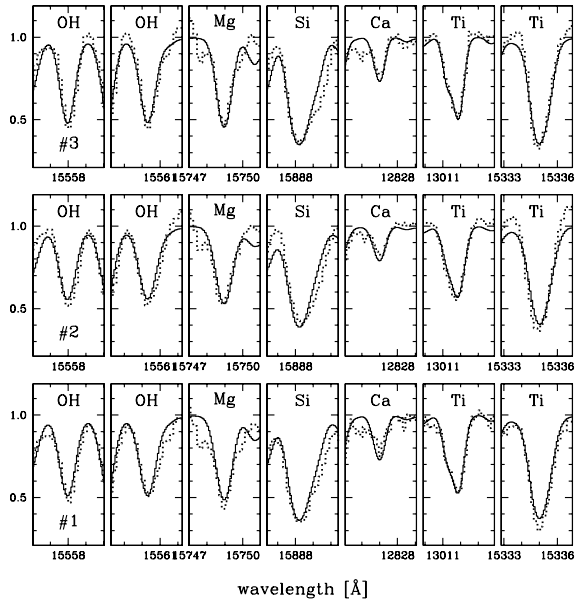

Fig. 3. GIANO spectra around some alpha element lines for the three observed RSG stars (dotted lines). Our best-fit models are overplotted as solid lines. Rest frame wavelengths are defined in air and thickmarks are every Å in each panel.

3. Chemical abundance analysis

Deriving chemical abundances of RSG stars is an intrinsically difficult task for several reasons, namely the high level of molecular blending and blanketing in their spectra, the degeneracy in the determination of surface parameters, and the various broadening effects due to micro and macro turbulence. The use of high-resolution spectroscopy in the NIR significantly mitigates the problem of the molecular blending and blanketing, which remains critical at optical wavelengths.

To measure chemical abundances from the GIANO spectra, we used full spectral synthesis techniques and equivalent width

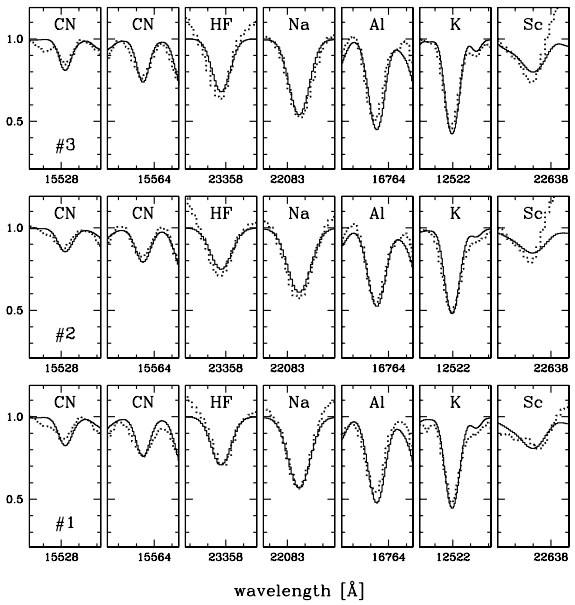

Fig. 4. GIANO spectra around some light element lines for the three observed RSG stars (dotted lines). Our best-fit models are overplotted as solid lines. Rest frame wavelengths are defined in air and thickmarks are every Å in each panel.

measurements of selected lines, sufficiently isolated, free from significant blending and/or contamination by telluric absorption and without strong wings. The presence of possible telluric absorption was carefully checked on an almost featureless O-star (Hip89584) spectrum.

We computed a large grid of suitable synthetic spectra to model RSG stars by varying the stellar parameters and the element abundances. We used the same code as in D09 to facilitate the comparison. This is an updated version (Origlia et al. 2002) of the program first described in Origlia et al. (1993).

The code was also successfully used to obtain abundances of bulge field (Rich et al. 2012, and references therein) and globular cluster (Origlia et al. 2008, and references therein) giants, young clusters dominated by RSGs (Larsen et al. 2006, 2008), and to study the chemical abundances of RSGs in the Galactic center (Davies et al. 2009a). The code uses the LTE approximation, is based on the molecular blanketed model atmospheres of Johnson et al. (1980) at temperatures ≤4000 K and on the ATLAS9 models for temperatures above 4000 K, and it includes thousands of NIR atomic transitions from the Kurucz database[1], Biemont & Grevesse (1973), and Melendez & Barbuy (1999), while molecular data are taken from our (Origlia et al. 1993, and subsequent updates) and Plez (priv. comm.) compilations. The reference solar abundances are taken from Grevesse & Sauval (1998).

Equivalent width measurements of the OH and CN molecular lines in the *H*-band, and of one HF line in the *K*-band were used to determine the oxygen, nitrogen and fluorine abundances. ^{12}C and ^{13}C carbon abundances were mostly determined from the CO bandheads in the *H* and *K*-bands, respectively, by means of full spectral synthesis, because of the high level of crowding and blending of the CO lines in these stars. Figure 5 shows the GIANO spectra of the three RSGs centered on some of the CO bandheads used for determining the carbon abundances and our best-fit models.

[1] http://www.cfa.harvard.edu/amp/ampdata/kurucz23/sekur.html

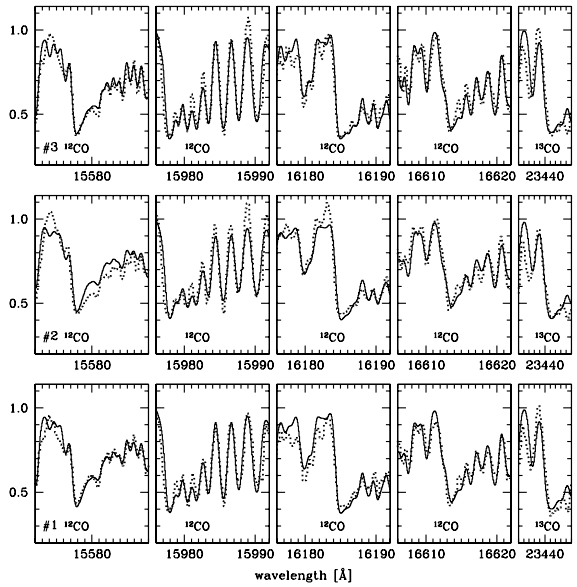

Fig. 5. GIANO H-band spectra of the ^{12}CO (3–0), (5–2), (6–3) and (8–5) bandheads and K-band spectra of the ^{13}CO (3–0) bandhead for the three observed RSG stars (dotted lines). Our best-fit models are overplotted as solid lines. Rest frame wavelengths are defined in air.

Equivalent width measurements of neutral atomic lines over the full spectral range covered by the GIANO spectra were used to derive abundances of Fe and other iron-peak elements such as V, Cr, Ni, of alpha (Mg, Si, Ca and Ti) and other light elements such as Na, Al, K, Sc, and of the s-process element Y, while Sr abundances were obtained from ionized lines. Table 3 (available online) reports the list of lines used in the present analysis and their measured equivalent widths.

Some other atomic lines of S (Y-band), Mn (J-band), Co, and Cu (H-band) are present in the spectra of the observed RSGs, but they are either too saturated or blended and/or contaminated by telluric absorption, which makes them ineffective for deriving reliable abundances.

This compilation is a first census of the usable lines for abundance analysis and it does not pretend to be complete. Work is in progress to identify other potential lines of interest that, however, will be checked on forthcoming observed spectra of less extreme stars for a proper calibration. We note that our compilation contains several lines in common with the Smith et al. (2013) APOGEE spectral line list.

We compared the observed spectra with models in which temperature, gravity, and microturbulence velocity are as carefully determined in D09, that is $T_{\rm eff}$ = 3600 K, log g = 0.0 and ξ = 2 km s^{-1} for all the three stars. These parameters were fine-tuned to enable simultaneous spectral fitting of the CO and OH molecular bands and the few atomic lines in the NIRSPEC spectra. The many more CO, OH, and CN molecualr lines as well as neutral atomic lines available in the GIANO spectra allowed us to carefully verify the reliability of the parameters adopted in D09. Models with these atmospheric parameters satisfactorily reproduce both the D09 and the current GIANO spectra. However, while D09 obtained good fits to the data without including an additional macroturbulence velocity broadening, since this was not resolved at their spectral resolution of $R \simeq 17\,000$, this is not the case for the GIANO spectra at $R \simeq 50\,000$. We obtained a good fit to the observed spectra by modeling macroturbulence velocity with a Gaussian σ broadening of about 6.4, 7.1, and 5.7 km s^{-1}, or equivalently Doppler-broadening of 9, 10, and 8 km s^{-1}, for stars #1, #2 and #3, respectively. We did not find other appreciable line broadening by stellar rotation.

Table 2. Chemical abundances of the RSG stars observed with GIANO.

Element	Atomic #	[X/H] (#1)	(#2)	(#3)	$n_{\rm lines}$
Fe	26	–0.26 ±0.05	–0.48 ±0.05	–0.37 ±0.06	13
V	23	–0.36 ±0.10	–0.43 ±0.10	–0.30 ±0.10	1
Cr	24	–0.25 ±0.11	–0.32 ±0.14	–0.15 ±0.10	4
Ni	28	–0.30 ±0.05	–0.47 ±0.07	–0.34 ±0.04	6
Mg	12	–0.19 ±0.13	–0.60 ±0.10	–0.33 ±0.08	5
Si	14	–0.12 ±0.03	–0.61 ±0.07	–0.40 ±0.05	7
Ca	20	–0.29 ±0.08	–0.48 ±0.07	–0.40 ±0.08	7
Ti	22	–0.19 ±0.07	–0.35 ±0.07	–0.28 ±0.06	21
C	6	–0.75 ±0.05	–0.85 ±0.05	–0.65 ±0.05	–
N	7	+0.23 ±0.04	+0.01 ±0.04	+0.07 ±0.03	18
O	8	–0.41 ±0.04	–0.41 ±0.06	–0.32 ±0.05	23
F	9	–0.23 ±0.10	–0.34 ±0.10	–0.11 ±0.10	1
Na	11	–0.01 ±0.20	–0.15 ±0.14	–0.27 ±0.11	2
Al	13	–0.32 ±0.08	–0.48 ±0.08	–0.35 ±0.06	3
K	19	–0.37 ±0.07	–0.55 ±0.05	–0.22 ±0.09	3
Sc	21	–0.22 ±0.09	–0.13 ±0.09	–0.07 ±0.06	2
Sr	38	– –	–0.25 ±0.06	–0.24 ±0.19	2
Y	39	–0.61 ±0.10	–0.67 ±0.12	–0.67 ±0.13	2
^{12}C/^{13}C	–	9 ±1	10 ±1	11 ±1	–

The final average abundances are quoted in Table 2 and plotted in Fig. 6. The impact of using slightly different assumptions for the stellar parameters on the derived abundances is discussed in Sect. 3.1.

Recently, Davies et al. (2013) discussed the problem of the most appropriate temperature scale for RSGs (see also Levesque et al. 2005), given that temperatures differing by several hundreds degrees can be inferred, using different scales. For the sake of consistency we therefore also explore models with significantly warmer ($T_{\rm eff}$ > 4000 K) and cooler ($T_{\rm eff}$ < 3200 K) temperatures than the one adopted in this analysis as best-fit value. We found that for temperatures above 3800K we were still able to fit the observed spectra by using very peculiar enhanced N and O abundances, providing unlikely [O/Fe] > 0.9 dex and [C+N/Fe] > 1.0 dex. For temperatures below 3200 K, we were barely (at >1.5 sigma level) able to fit the spectra with very peculiar depleted N and O abundances, providing [O/Fe] < −0.3 dex and [C+N/Fe] ≈ −0.5 dex. The impact on the overall iron and iron-peak elemental abundances is much weaker (within 0.1–0.2 dex).

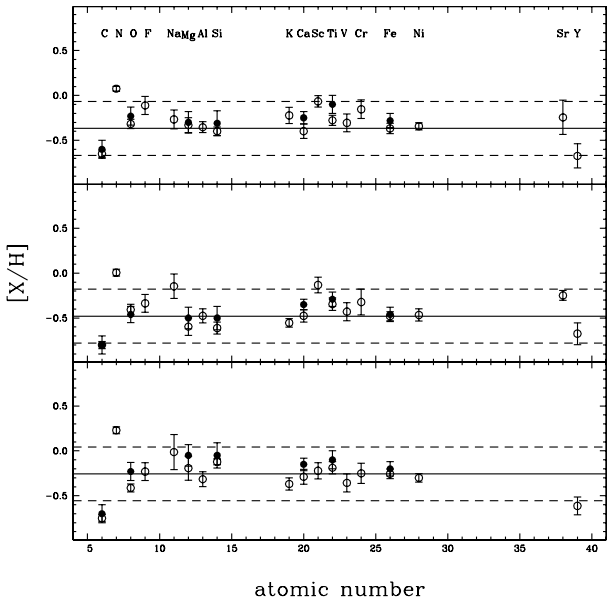

Fig. 6. Open circles: [X/H] chemical abundances as a function of the atomic number for the three RSGs observed with GIANO. Solid dots: corresponding [X/H] abundances from D09. The horizontal lines mark the [Fe/H] abundance (solid line) and the ±0.3 dex values (dashed lines), as inferred in the present analysis.

3.1. Error budget

We can quantify random and systematic errors in the measurements of the equivalent widths and in the derived chemical abundances as follows: the typical random error of the measured line equivalent widths is between 10 and 20 mÅ, mostly arising from a ±2% uncertainty in the placement of the pseudo-continuum, as estimated by overlapping the synthetic and the observed spectra. These random uncertainties in the line equivalent width measurements correspond to abundance variations ranging from a few hundredths to 1 tenth of a dex. This ≤0.1 dex error is lower than the typical 1σ scatter in the derived abundances from different lines, which normally ranges between 0.1 and 0.2 dex. The errors quoted in Table 2 for the final abundances were obtained by dividing these 1σ errors by the squared root of the number of used lines, ranging from a few to about 20. A 10–20 mÅ variation of line equivalent width value was also obtained by varying the Gaussian line broadening (due to macro turbulence) by ≃1 km s^{-1}, but this is mostly a systematic effect.

The other systematics arise from varying the adopted stellar parameters. To properly quantify them, we generated a grid of test models with $T_{\rm eff}$ between 3400 K and 3800 K, log g between 0.0 and 1.0 dex, and ξ between 2 and 4 km s^{-1}.

We found that variations of ±100 K with respect to the adopted temperature of 3600 K have a weak effect on the measured equivalent widths of atomic lines (on average the variation is <10 mÅ corresponding to a variation of few hundredths dex of the element abundance). Molecular OH and CN lines are more sensitive to temperature variations: their equivalent widths can vary by 15–20 mÅ by varying temperature of ±100 K, corresponding to ≤0.1 dex variation of the element abundance. A variation of log g by ±0.5 dex has a negligible impact on the equivalent width of the OH lines, while it produces a variation of ≃20 mÅ (≃0.15 dex in abundance) and ≃30 mÅ (≃0.20 dex in abundance) in the equivalent widths of the atomic and CN lines, respectively. A variation of ξ by ±0.5 km s^{-1} has a negligible impact on the equivalent widths of CN lines, while it produces a variation of ≃15–20 mÅ in the equivalent widths of atomic and OH lines, corresponding to a variation of ≤0.1 dex of the element abundance. A somewhat conservative estimate of the overall systematic uncertainty in the abundance (A) determination, caused by variations of the atmospheric parameters, can be computed as follows: $(\Delta A)^2 = (\partial A/\partial T)^2(\Delta T)^2 + (\partial A/\partial \log g)^2(\Delta \log g)^2 + (\partial A/\partial \xi)^2(\Delta \xi)^2$ and it amounts to 0.15–0.20 dex.

We also determined the statistical significance of our best-fit solution for the spectral synthesis of the CO features and the derived carbon abundances. As a figure of merit of the statistical test we adopted the difference between the model and the observed spectrum. To quantify systematic discrepancies, this parameter is more powerful than the classical χ^2 test, which is instead equally sensitive to *random* and *systematic* scatters (see Origlia & Rich 2004, for more discussion and references).

Our best-fit solutions always show >90% probability to be representative of the observed spectra, while those with ±0.1 dex carbon abundance are significant at ≥1.5σ level only.

We also computed other test models with $\Delta T_{\rm eff}$ = ±200 K, $\Delta \log g$ = ±0.5 dex and $\Delta\xi$ = ±0.5 km s^{-1}, and also with corresponding simultaneous variations of the C abundance (0.1–0.2 dex) to reproduce the depth of the molecular features. CO molecular bands are very sensitive thermometers in the range of temperature between 4500 K and 3800 K. Indeed, temperature sets the fraction of molecular *versus* atomic carbon. At temperatures below 3800 K most of the carbon is in molecular form, which drastically reduces the dependence of the CO band strengths on the temperature itself. At temperatures ≥4500 K molecules barely survive, most of the carbon is in atomic form, and the CO spectral features become very weak. Solutions with $\Delta \log g$ = ±0.5 dex or with $\Delta\xi$ = ±0.5 km s^{-1} and corresponding 0.1–0.2 dex variation of the carbon abundance are significant at ≥1.5σ level only.

4. Results and discussion

The abundances of all chemical elements with measurable lines in the GIANO spectra are very similar in all the three RSGs, as expected because they are members of a star cluster.

We found iron abundances between half and one third solar, in good agreement with the previous estimates by D09. The other iron-peak elements (V, Cr, Ni) show abundances that are consistent with the iron values to within ±0.15 dex, thus fully confirming the sub-solar metallicity of the cluster.

The alpha (O, Mg, Si, Ca, Ti) as well as most of the other light (F, Na, Al,K, Sc) elements behave in a similar fashion, with [X/Fe] abundance ratios about solar (±0.15 dex); the only exceptions are [F/Fe] and [Sc/Fe] in star #1, [Na/Fe] in star #2 and [Na/Fe] and [Sc/Fe] in star #3, which are slightly enhanced (but always within a factor of two).

Interestingly, the measured [F/O] abundance ratios (+0.18 in star #1, +0.07 in star #2 and +0.21 in star #3), are fully consistent with the values measured in K-M dwarfs in the Orion Nebula Cluster by Cunha & Smith (2005) and are representative of the disk composition.

The Sr and Y s-process elements behave somewhat differently from each other: [Sr/Fe] is slightly enhanced, while [Y/Fe] is slightly depleted (by a factor of ≤2) with respect to solar.

[C/Fe] is depleted by a factor between two and three, similarly to what was found by D09, and the $^{12}C/^{13}C$ ratio is also rather low (between 9 and 11), indicating that some extra-mixing processes in the stellar interiors are at work during the post-main-sequence evolution. Evolutionary tracks of massive stars with rotation (e.g. Meynet & Maeder 2000) can account for both

the overall depletion of carbon and the low $^{12}C/^{13}C$ isotopic ratio, and indeed, deep, rotationally enhanced mixing was previously suggested by D09.

[N/Fe] is enhanced in such a way that [C+N/Fe] is about 0.0 (+0.00 in star #1, +0.12 in star #2, and +0.16 in star #3), consistent with standard CN nucleosynthesis.

The mostly solar-scaled [X/Fe] abundance patterns of iron-peak, alpha, and other light elements as measured in the observed three RSGs of RSCG2 are fully consistent with the chemistry of the thin disk (see e.g. Reddy et al. 2003), that underwent chemical enrichment over long timescales with the contribution of both type II and type I supernovae. At variance, the sub-solar metallicity of RSGC2 and of its companion cluster RSGC1 (see D09) is intriguing. Indeed, abundance measurements of Cepheids in the inner disk (see e.g. Genovali et al. 2013; Andrievsky et al. 2013, and references therein) indicate the existence of a positive metallicity gradient toward the inner regions and metal abundances well in excess of solar. However, these measurements still sample a region at a minimum Galactocentric distance of about 4 kpc because of the huge extinction closer to the center. Only a few IR measurements of RSGs exist so far in the innermost disk region and in the Galactic center (e.g. Ramirez et al. 2000; Martins et al. 2008; Najarro et al. 2009; Davies et al. 2009a,b), consistent with a metal abundance of about solar and some level of alpha-element enhancement (see e.g. Cunha et al. 2007).

It is therefore clear that neither RSGs in the Scutum star clusters (D09 and the present work) nor RSGs in the center of the Galaxy follow the radial Galactic trend traced by Cepheids and other young stellar populations at Galactocentric distances RGC $>$ 3−4 kpc (see D09 and Genovali et al. 2013, for more discussion and references). However, this is not surprising, because the innermost region of the Galaxy shows several different substructures, such as the bulge/bar and the ends of the spiral arms, with strong fluctuations in stellar/gas density and star formation rates. In such a complex physical and kinematic environment, the chemical enrichment process is also expected to have been quite inhomogeneous.

5. Conclusions

As a preliminary test of the scientific performances of the GIANO spectrograph during its first commissioning in July 2012, we observed three bright RSGs in the Scutum star cluster RSGC2.

A NIR spectrograph such as GIANO, which provides high spectral resolution and full spectral coverage in a single exposure, is a unique instrument to perform detailed chemical studies of cool stars in any Galactic environment, including highly reddened star clusters such as RSGC2 in the inner Galactic disk.

The high spectral resolution has allowed us to resolve and measure the macro turbulence broadening in the observed RSGs and to better identify unblended lines for accurate equivalent width measurements and chemical abundance determinations.

The simultaneous access to the *YJH* and *K*-bands offers the possibility of sampling most of the elements of interest for a complete check of the chemical clock and of measuring from a few to several tens of lines per element, thus enabling an accurate and statistically significant abundance analysis. We used the *Y*-band to measure Cr and Sr, the *J*-band to measure K and some Fe, Cr, Ca, Mg, Si, and Ti lines, the *H*-band to measure ^{12}C, N, O, Al, V, and Ni, most of the Fe lines and some Al Ca, Mg, Si and Ti lines, and finally the *K*-band to measure ^{13}C, F, Na, Sc, Y and a few Al, Ti and Fe lines.

For the three observed RSGs we found overall abundance patterns consistent with the thin-disk chemistry, and we confirmed the sub-solar metallicity of the RSGC2 star cluster, as previously suggested by D09, which indicates that the inner disk in particular, but more generally the inner Galaxy, has quite an inhomogeneous chemical composition.

Acknowledgements. Part of this work was supported by the grant TECNO-INAF-2011. This publication makes use of data products from the Two Micron All Sky Survey, which is a joint project of the University of Massachusetts and the Infrared Processing and Analysis Center/California Institute of Technology, funded by the National Aeronautics and Space Administration and the National Science Foundation. We thank Ben Davies for his carefull referee report.

References

Andrievsky, S. M., Lepine, J. R. D., Korotin, S. A., et al. 2013, MNRAS, 428, 3252
Biemont, E., & Grevesse, N. 1973, Atomic Data and Nuclear Data Tables, 12, 221
Davies, B., Figer, D. F., Kudritzki, R., et al. 2007, ApJ, 671, 781
Davies, B., Origlia, L., Kudritzki, R., et al. 2009a, ApJ, 694, 46
Davies, B., Origlia, L., Kudritzki, R., et al. 2009b, ApJ, 696, 2014
Davies, B., Kudritzki, R., Plez, B., et al. 2013, ApJ, 767, 3
Cunha, K., & Smith, V. V. 2005, ApJ, 626, 425
Cunha, K., Sellgren, K., Smith, V. V., et al. 2007, ApJ, 669, 1011
Genovali, K., Lemasle, B., Bono, G., et al. 2013, A&A, 554, A132
Grevesse, N., & Sauval, A. J. 1998, Space Sci. Rev., 85, 161
Johnson, H. R., Bernat, A. P., & Krupp, B. M. 1980, ApJS, 42, 501
Kramida, A., Ralchenko, Yu., Reader, J., & NIST ASD Team 2012, NIST Atomic Spectra Database (version 5.0), http://physics.nist.gov/asd
Larsen, S. S., Origlia, L., Brodie, J., & Gallagher, J. S. 2006, MNRAS, 368, 10
Larsen, S. S., Origlia, L., Brodie, J., & Gallagher, J. S. 2008, MNRAS, 383, 263
Levesque, E. M., Massey, P., Olsen, K. A. G., et al. 2005, ApJ, 628, 973
Martins, F., Hillier, D. J., Paumard, T., et al. 2008, A&A, 478, 219
Meynet, G., & Maeder, A. 2000, A&A, 361, 101
Melendez, J., & Barbuy, B. 1999, ApJS 124, 527
Najarro, F., Figer, D. F., Hillier, D. J., Geballe, T. R., & Kudritzki, R. P. 2009, ApJ, 691, 1816
Oliva, E., Origlia, L., Maiolino, R., et al. 2012a, SPIE, 8446, 3
Oliva, E., Biliotti, V., Baffa, C., et al. 2012b, SPIE, 8453, 2
Oliva, E., Origlia, L., Maiolino, R., et al. 2013, A&A, 555, A78
Origlia, L., & Rich, R. M. 2004, AJ, 127, 3422
Origlia, L., Moorwood, A. F. M., & Oliva, E. 1993, A&A, 280, 536
Origlia, L., Rich, R. M., & Castro, S. 2002, AJ, 123, 1559
Origlia, L., Valenti, E., & Rich, R. M. 2008, MNRAS, 388, 1419
Ramirez, S. V., Sellgren, K., Carr, J. S., et al. 2000, ApJ, 537, 205
Reddy, B. E., Tomkin, J., Lambert, D. L., & Allende Prieto, C. 2003, MNRAS, 340, 304
Redman, S. L., Lawler, J. E., Nave, G., Ramsey, L. W., & Mahadevan, S. 2011, ApJS, 195, 24
Rich, R. M., Origlia, L., & Valenti, E. 2012, ApJ, 746, 59
Smith, V. V., Cunha, K., Shetrone, M. D., et al. 2013, ApJ, 765, 16
Verheyen, L., Messineo, M., & Menten K. M. 2012, A&A, 541, A36

Pages 7 to 8 are available in the electronic edition of the journal at http://www.aanda.org

Table 3. Lines identified in the RSG stars observed with GIANO.

λ_{air} μm	log gf	χ eV	EW(#1) mÅ	EW(#2) mÅ	EW(#3) mÅ
Fe I lines					
1.22133	–1.94	4.64	133	88	93
1.22271	–1.46	4.61	160	140	146
1.23429	–1.56	4.64	186	151	139
1.26159	–1.61	4.64	131	127	128
1.28249	–4.19	3.02	193	170	151
1.28406	–1.47	4.96	134	140	152
1.52075	0.23	5.39	378	360	336
1.52450	–0.28	5.59	349	302	303
1.53947	–0.12	5.62	360	370	333
1.53957	–0.26	5.62	296	284	291
1.57694	0.60	5.54	469	466	403
1.59649	–0.08	5.92	268	269	263
2.23808	–0.46	5.04	447	424	410
V I lines					
1.67577	–1.37	3.41	296	291	288
Cr I lines					
1.06721	–1.37	3.02	212	189	256
1.08014	–1.72	3.01	188	195	182
1.09059	–0.65	3.44	217	248	215
1.25218	–1.59	2.71	379	383	327
Ni I lines					
1.55554	0.07	5.49	320	272	271
1.63105	0.07	5.29	333	338	299
1.63642	0.44	5.29	474	482	454
1.65893	–0.49	5.47	156	159	161
1.69967	0.31	5.31	339	337	295
1.70016	0.23	5.49	250	217	219
Mg I lines					
1.18282	–0.29	4.35	392	402	377
1.57407	–0.24	5.94	419	382	374
1.57490	–0.06	5.94	486	452	405
1.57658	0.38	5.94	490	482	434
1.59545	–1.03	6.59	287	239	249
Si I lines					
1.19916	–0.16	4.92	308	258	241
1.21035	–0.39	4.93	283	278	247
1.22707	–0.41	4.96	279	248	240
1.58884	–0.03	5.09	554	567	493
1.59601	0.13	5.99	417	386	370
1.60600	–0.44	5.96	311	239	285
1.60948	–0.11	5.97	371	315	324
Ca I lines					
1.28160	–0.63	3.91	220	222	199
1.28239	–0.85	3.91	209	221	219
1.28271	–1.33	3.91	157	124	117
1.61508	0.36	5.30	364	354	331
1.61552	–0.02	5.30	277	211	218
1.61574	0.49	5.32	327	287	289
1.61971	0.64	5.30	439	406	363
Ti I lines					
1.17805	–2.38	1.44	296	241	224
1.17972	–2.46	1.43	289	309	273
1.18929	–1.91	1.43	326	356	305
1.19495	–1.76	1.44	303	328	279
1.23884	–2.20	2.16	166	134	135
1.25696	–2.26	2.18	205	167	208
1.26711	–2.52	1.43	244	322	304
1.27384	–1.39	2.18	258	283	262
1.27449	–1.35	2.49	259	220	190
1.28217	–1.53	1.46	411	439	360
1.28314	–1.11	1.43	382	381	349
1.28470	–1.55	1.44	382	401	355
1.29199	–1.22	2.15	258	209	226
1.29876	–1.78	2.51	143	167	161
1.30054	–2.46	2.18	161	155	173
1.30119	–2.49	1.44	313	317	280
1.53348	–1.15	1.89	596	608	512
1.55438	–1.48	1.88	558	580	497
2.17829	–1.16	1.75	735	726	648
2.18974	–1.45	1.74	644	615	595
2.24439	–2.25	1.74	536	478	486
Al I lines					
1.67190	0.15	4.09	477	478	446
1.67634	–0.55	4.09	421	423	394
2.10930	–0.31	4.09	509	503	475
Na I lines					
2.20837	–0.02	3.19	538	548	494
2.33791	0.53	3.76	566	563	489
K I lines					
1.17728	0.51	1.62	293	287	292
1.24323	–0.44	1.61	222	234	244
1.25221	–0.14	1.62	358	353	318
Sc I lines					
2.17305	–1.68	1.44	447	513	490
2.26370	–2.17	1.44	313	367	337
Sr II lines					
1.03273	–0.35	1.84	–	387	325
1.09149	–0.64	1.81	–	383	344
Y I lines					
2.12604	–0.10	1.43	419	446	417
2.25438	–0.20	1.40	–	362	346
$^{12}C^{14}N$ lines					
1.52132	–2.00	0.83	198	194	197
1.52195	–1.80	0.73	313	287	267
1.52604	–1.35	0.92	235	195	180
1.52689	–1.41	1.29	161	123	121
1.52726	–1.57	0.77	202	174	162
1.52916	–1.92	0.85	144	162	135
1.53071	–1.90	0.85	168	166	162
1.53214	–1.75	0.79	203	183	168
1.53974	–1.80	0.91	227	211	177
1.54396	–1.77	0.93	184	193	176
1.54471	–1.16	1.09	217	214	196
1.54662	–1.15	1.09	238	230	205
1.55282	–1.71	1.00	143	117	126
1.55634	–1.14	1.15	219	139	193
1.56093	–1.51	0.94	217	199	203
1.56136	–1.14	1.18	282	225	224
1.56736	–1.65	1.07	288	207	221
1.56749	–1.65	1.09	208	164	198
$^{16}O^{1}H$ lines					
1.51458	–5.63	0.16	425	478	427
1.51479	–5.63	0.16	391	461	400
1.52366	–5.93	0.45	260	349	238
1.53285	–5.67	0.47	451	441	378
1.53912	–5.59	0.49	330	354	325
1.54092	–5.55	0.26	376	451	401
1.54698	–5.26	0.94	220	250	309
1.54969	–5.26	0.91	302	306	267
1.55053	–5.46	0.52	358	438	383
1.55580	–5.49	0.30	452	461	417
1.55602	–5.49	0.30	422	455	418

Notes. Wavelengths are defined in air ($\lambda_{air} = \lambda_{vacuum}/1.000274$). We also list the line transition probability (log gf), excitation potential (χ) and the measured equivalent widths in the three observed RSG stars.

Table 3. continued.

λ_{air} μm	log gf	χ eV	EW(#1) mÅ	EW(#2) mÅ	EW(#3) mÅ
1.55658	–5.42	0.90	234	227	228
1.55688	–5.45	0.30	395	432	409
1.55721	–5.45	0.30	418	463	418
1.56519	–5.29	0.53	324	270	273
1.56535	–5.29	0.53	389	366	345
1.58977	–5.36	0.41	442	465	434
1.59104	–5.14	0.60	359	338	357
1.59127	–5.14	0.60	370	373	363
1.63522	–5.00	0.74	448	442	442
1.63546	–5.00	0.74	365	333	353
1.63681	–4.96	0.73	359	331	368
1.68723	–5.15	0.76	372	353	388
$^{1}H^{9}F$ lines					
2.33577	–3.95	0.48	372	353	388